MNRAS **000**, 1–8 (2019) Preprint 20 May 2019 Compiled using MNRAS LATEX style file v3.0

Rotational and pulsational variability in the *TESS* light curve of HD 27463

V. Khalack[1], C. Lovekin[2], D. M. Bowman[3], O. Kobzar[1], A. David-Uraz[4], E. Paunzen[5], J. Sikora[6,7], P. Lenz[8]

[1]*Département de Physique et d'Astronomie, Université de Moncton, Moncton, N.B., Canada E1A 3E9*
[2]*Department of Physics, Mount Allison University, Sackville, N.B., Canada E4L 1E6*
[3]*Institute of Astronomy, KU Leuven, Celestijnenlaan 200D, 3001 Leuven, Belgium*
[4]*Department of Physics & Astronomy, University of Delaware, 217 Sharp Lab, Newark, DE 19716, USA*
[5]*Department of Theoretical Physics and Astrophysics, Masaryk University, Kotlářská 2, 611 37 Brno, Czech Republic*
[6]*Department of Physics, Engineering Physics & Astronomy, Queen's University, Kingston, ON, Canada K7L 3N6*
[7]*Department of Physics and Space Physics, Royal Military College of Canada, PO Box 17000 Kingston, ON, Canada K7K 7B4*
[8]*Ronin Institute, Montclair, NJ 07043, USA*

Accepted ???. Received ???; in original form ???

ABSTRACT

The new photometric data on HD 27463 obtained recently with the Transiting Exoplanet Survey Satellite (*TESS*) are analysed to search for variability. Our analysis shows that HD 27463 exhibits two types of photometric variability. The low frequency variability with the period P= 2.834274 $\pm$ 0.000008 d can be explained in terms of axial stellar rotation assuming the oblique magnetic rotator model, while the detected high-frequency pulsations characterise this object as a δ Scuti variable. From the analysis of Balmer line profiles visible in two FEROS spectra of HD 27463 we have derived its effective temperature and surface gravity that are close to the values published for this star in the *TESS* Input Catalogue (TIC). Knowing the period of axial stellar rotation and vsin i value estimated from the fitting of Balmer line profiles we found that the rotational axis is inclined to the line of sight at the angle $i = 33 \pm 8$ deg. Our best fitting model of the observed pulsation modes results in the overshoot of $f_{ov} = 0.016$ and the values of global stellar parameters that are well consistent with the data reported in the TIC and with the data derived from the simulation of Balmer line profiles. This model indicates an age of 4.991 $\times 10^8$ years, which corresponds to a core hydrogen fraction of 0.332.

Key words: stars: magnetic field – stars: rotation – stars: oscillations – stars: fundamental parameters – stars: chemically peculiar – stars: individual: HD 27463

1 INTRODUCTION

Ever since a strong peculiarity was discovered in the Si II doublet of the archetypal star α^2 CVn (Maury & Pickering 1897), chemically peculiar stars have been the subject of numerous studies. In particular, Ap stars (classified as 'CP2' in contrast to Am, HgMn or He stars) are known to exhibit periodic brightness variations generally understood to be associated with rotation taking into account that in these stars, strong magnetic fields (Babcock 1958) lead to the creation of surface abundance patches.

A subset of Ap stars lie within the δ Scuti instability strip. Accordingly, high frequency pulsational signatures have been discovered in a number of Ap stars, starting with Przybylski's star (HD 101065; Kurtz 1978). Dedicated surveys have revealed a few rapidly oscillating Ap (or 'roAp') stars, but were limited to fairly high amplitude pulsations since they were carried out using ground-based observations. However, dedicated ground-based surveys (e.g. Holdsworth et al. 2014), and the advent of high-precision space-based photometry has enabled the discovery of new Ap pulsators (e.g. HD 24355 and HD 137949, discovered using K2 observations; Holdsworth et al. 2016, 2018).

The Transiting Exoplanet Survey Satellite (*TESS*) was launched by NASA on 18 April 2018 with the purpose of detecting exoplanets using the transit method (Ricker et al. 2015). Over the course of its 2-year nominal mission, it will cover most of the sky in 26 sectors with its four wide-field cameras, each covering 24×24 deg. Each sector is observed for $\sim$27 d, and sectors in each celestial hemisphere overlap near the pole; therefore stars observed by *TESS* will have temporal baselines between 27 d and about a year. All fields are observed with a 30-minute cadence (in full-frame images, or FFIs) but a subset ($> 200,000$) of stars have been selected for short-cadence (2 min) observations, forming the candidate target list (CTL; Stassun et al. 2018). With such a temporal

baseline and cadence, *TESS* not only represents a formidable asset for exoplanetary detection, but can also be leveraged very profitably for asteroseismology (e.g. Campante et al. 2016). As such, this mission represents a tremendous opportunity to not only significantly increase the sample size of known pulsating Ap stars (see e.g. Cunha et al. 2019), but also, given the exquisite data quality, to perform a detailed characterization of specific objects of interest.

The chemically peculiar (CP) star HD 27463 (TT Ret, HIP 19917, Renson 7050, TIC 38586082) is known as an α^2 CVn type variable with spectral type ApEuCr(Sr) (Houk & Cowley 1975). Photometric variability of this star with a period of P = 2.83507 ± 0.00008 days and the epoch of E = 2448502.2944±0.0004 has been reported in the Hipparcos-2 catalogue (van Leeuwen 2007).

HD 27463 is a long period (∼370 years) visual binary (separation of ∼0.3”), with a difference of magnitude between the Ap primary and the secondary of about 0.43 in the *V* band (e.g. Baize & Petit 1989 and references therein). Previous surveys designed to detect high frequency pulsations did not yield any detection in this star (Martinez & Kurtz 1994; Joshi et al. 2016). However, using *TESS* data, Cunha et al. (2019) and Sikora et al. (2019) have classified HD 27463 as a suspected new δ Scuti variable. Therefore, in this study, we set out to perform a more involved investigation of this star’s (*TESS* photometry, in conjunction with high-resolution spectroscopy. This study is carried out as part of the MOBSTER collaboration, an analysis of magnetic O, B and A stars (David-Uraz et al. 2019), and of the VeSElkA project, a search for CP stars with vertical stratification of elements abundance (Khalack & LeBlanc 2015a,b).

The photometric and spectral observations and the respective reduction procedures are described in Section 2. The use of automatic software to analyse the light curves is considered in Section 3. Comparison of the fundamental stellar parameters derived from the analysis of Balmer line profiles and from the simulation of stellar pulsation are shown in Section 4. The discussion follows in Section 5.

2 OBSERVATIONS AND DATA REDUCTION

HD 27463 has been observed by *TESS* in Sectors 1–5 in the frame of the *TESS* guest program Rotationally-Induced Variability Of Chemically Peculiar (CP) Stars (Ricker & Vanderspek 2018). The *TESS* data products have been reduced employing the SPOC pipeline (Jenkins et al. 2016), which is based on the Kepler Science Processing Pipeline. The light curves and the associated data listed in the *TESS* Input Catalogue (TIC[1]) have been downloaded via the Mikulski Archive for Space Telescopes (MAST[2]) and are publicly available. The extracted time series of flux measurements taken at different Barycentric Julian Dates (BJD) were transformed to units of stellar magnitude. The light curves have been normalised to be zero in the mean.

To accurately determine the rotation period and the pulsation mode frequencies of HD 27463, we further detrended the 2-min *TESS* light curve following the methodology of Bowman et al. (2018b). We fit a periodic rotational modulation model comprising multiple harmonics of the rotation frequency, $\nu_{rot} = 0.352824 \pm 0.000001$ d^{-1}, to the light curve using non-linear least-squares. We

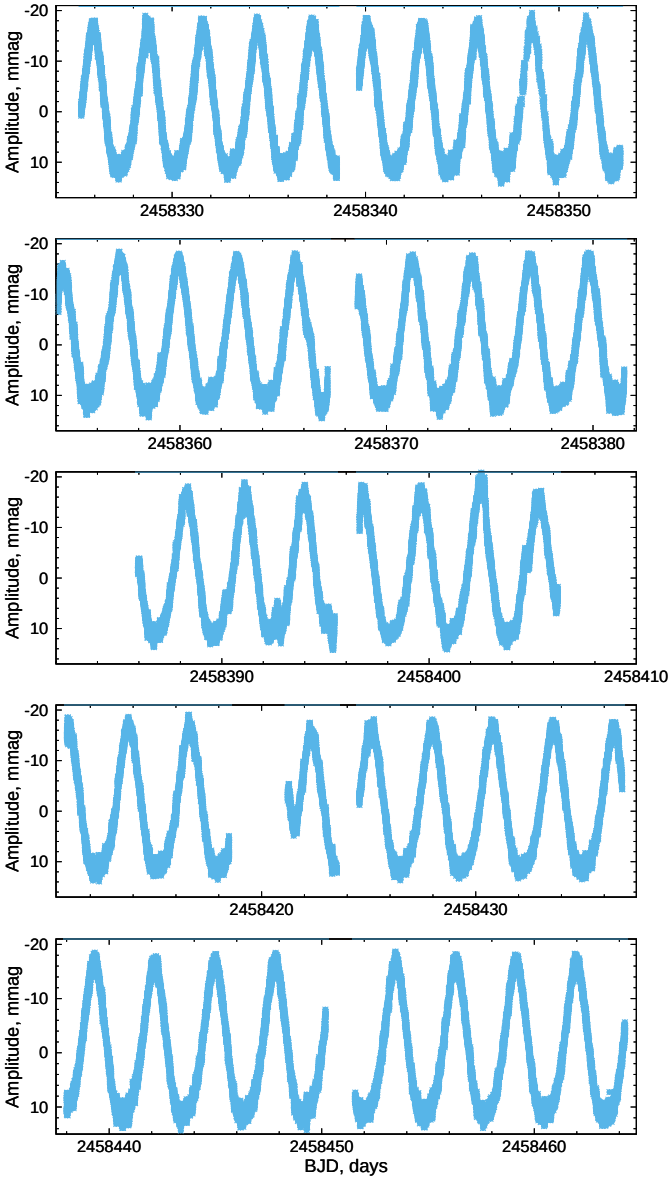

Figure 1. Examples of the detrended light curves obtained by *TESS* for HD 27463 in Sectors 1-5 (from top to bottom).

subsequently subtracted this preliminary fit and modeled the residuals using a locally weighted scatterplot smoothing (LoWeSS) filter (Cleveland 1979; Seabold & Perktold 2010). To create our final detrended light curve, we subtracted the modelled residuals from the original light curve. This ensures that a high-quality light curve is used for the determination of a rotation period and for the extraction of pulsation mode frequencies, since the long-period and instrumental systematics have been removed.

HD 27463 has been observed twice in 2008 with the spectrograph FEROS installed on the 2.2 m Max Planck Gesellschaft/European Southern Observatory (MPG/ESO) telescope in La Silla. The spectrograph FEROS provides high-resolution spectra with R∼ 48000 in the spectral region from 3600 to 9200Å (Kaufer et al. 1999). Two available spectra of HD 27463 were reduced with the ESO automatic reduction pipeline employing the barycentric velocity correction. Nowadays the spectra are pub-

[1] https://archive.stsci.edu/tess/tic_ctl.html
[2] http://archive.stsci.edu/tess/all products.html

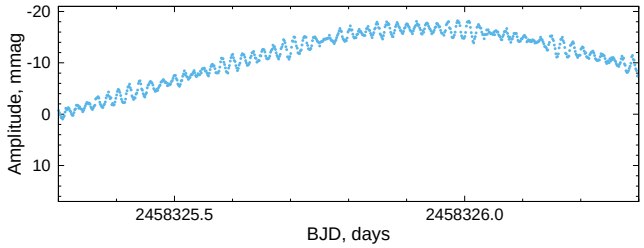

Figure 2. Part of the light curves obtained with *TESS* for HD 27463 over a time span of 1 day in Sector 1. The observed long-term variability is related to the stellar rotation (see Fig. 1). Stellar pulsations with frequencies expected from a δ Scuti variable and beating of close pulsation frequencies are clearly visible (see also the lower panel in Fig. 3).

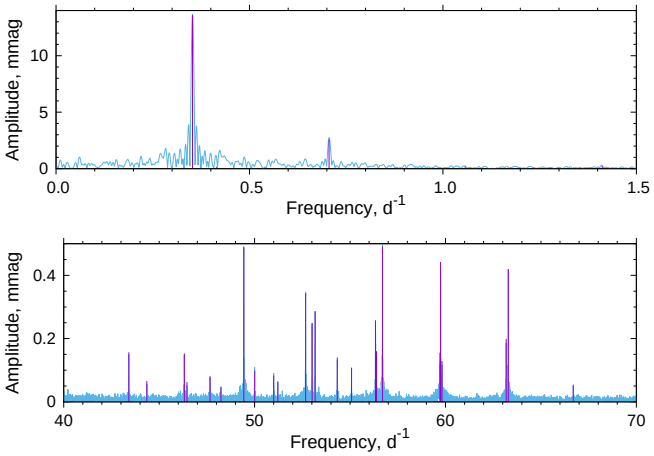

Figure 3. Examples of periodograms derived from analysis of HD 27463 light curves at the low (upper panel) and high (bottom panel) frequencies. Variability at the low frequencies is related to axial rotation of the star, while signals detected at the high frequencies are due to stellar pulsations.

lic and have been downloaded from the ESO archive[3]. To carry out analysis of Balmer line profiles we have used non-normalized spectra (see Section 4) and therefore no additional reduction procedure has been applied to the downloaded data.

3 PHOTOMETRIC ANALYSIS

To carry out the analysis of *TESS* light curves we have developed an automatic software (several scripts and codes including the code PERIOD04) that treats time series, performs periodic analysis, extracts data for a studied star from the public astronomical databases (TIC, SIMBAD, GALAH), prepares images and a list of found periodicities, and stores all the information in a final report.

The code PERIOD04 (version 1.2.9) developed by Lenz & Breger (2005) has been specially designed to carry out a statistical analysis of large astronomical data sets with significant gaps and is a powerful tool for identification and evaluation of periodic signals in long time series of stellar flux measurements. It has been recently modified by one of us (PL) to work in the *batch* mode such that it can be launched automatically from a script with a list of specified parameters. The significant peaks in the TESS light curve of HD 27463 have been extracted using the standard procedure of iterative pre-whitening and optimised using a multi-frequency least-squares fit procedure (Lenz & Breger 2005). This analysis yielded the detection of multiple frequencies with amplitudes having a significant signal-to-noise ratio. Significant peaks are defined as those with an amplitude larger than four times the level of noise left after pre-whitening the signal at the area of each studied frequency.

Finally, the combined light curve was fitted taking into account all detected frequencies using the least-squares procedure and the obtained periods, amplitudes and phases are shown respectively in the first, second and third columns of the Table 1. The presented uncertainties are the highest ones obtained from the error-matrix produced by the Levenberg-Marquardt non-linear least-squares fitting procedure and from the Monte Carlo simulation of a signal with the detected frequencies (Lenz & Breger 2005). They do not take into account the estimation errors reported for the flux measurements. In this approach the uncorrelated uncertainties for the frequency and the phase have been derived (Montgomery & Odonoghue 1999).

Table 1. Characteristics of the periodic signals detected in HD 27463 light curves from the first five sectors.

	Frequency, d^{-1}	Amplitude, mmag	Phase, rad/2π	S/N	Modes ℓ	m
ν_1	0.352824±0.000001	13.596± 0.006	0.9359±0.0001	29.1		
$2\nu_1$	0.705639±0.000006	2.573± 0.007	0.0895±0.0004	6.6		
	43.409828±0.000094	0.157± 0.007	0.9349±0.0279	14.5	2	2
	44.356363±0.000223	0.066± 0.013	0.9012±0.0557	6.3	3	0
	46.318147±0.000096	0.153± 0.007	0.8000±0.0065	14.2	2	-1
	46.456655±0.000235	0.062± 0.006	0.6032±0.0175	5.8	2	0
	47.667615±0.000181	0.081± 0.006	0.7426±0.0127	7.6	3	0
	48.238558±0.000322	0.046± 0.007	0.4482±0.0228	4.1	1	0
	49.433689±0.000030	0.491± 0.008	0.3511±0.0022	29.4	2	-1
	50.002473±0.000149	0.098± 0.006	0.8432±0.0115	5.9	2	1
	50.999734±0.000177	0.083± 0.007	0.7933±0.0123	8.1	3	0
	51.215952±0.000226	0.065± 0.006	0.6727±0.0147	6.6	3	0
	52.672629±0.000043	0.343± 0.006	0.1683±0.0032	18.9	2	-2
	53.012605±0.000059	0.248± 0.006	0.4302±0.0048	14.0	2	0
	53.173059±0.000051	0.286± 0.006	0.0920±0.0038	16.0	2	0
	54.333293±0.000105	0.140± 0.007	0.4882±0.0067	13.7	3	0
	55.076921±0.000137	0.107± 0.007	0.7837±0.0089	9.7	1	0
	56.332132±0.000057	0.258± 0.006	0.8862±0.0046	12.2	2	0
	56.337529±0.000080	0.183± 0.007	0.6321±0.0054	8.6	2	0
	56.383938±0.000092	0.160± 0.007	0.6144±0.0060	7.6	2	0
	56.700889±0.000030	0.491± 0.007	0.9475±0.0021	23.3	0	0
	56.700889±0.000030	0.491± 0.007	0.9475±0.0021	23.3	2	2
	59.709581±0.000095	0.155± 0.006	0.4958±0.0066	9.4	2	1
	59.741600±0.000033	0.442± 0.012	0.2427±0.0043	26.7	2	0
	59.746637±0.000155	0.095± 0.013	0.4808±0.0097	5.7	2	0
	59.815711±0.000114	0.129± 0.007	0.7050±0.0076	7.8	2	1
	63.180209±0.000074	0.199± 0.009	0.5228±0.0058	12.8	0	0
	63.290656±0.000035	0.420± 0.007	0.7557±0.0025	26.9	2	2
	66.696167±0.000283	0.052± 0.007	0.9038±0.0236	6.5	2	2

[3] http://archive.eso.org/wdb/wdb/adp/phase3_spectral/query

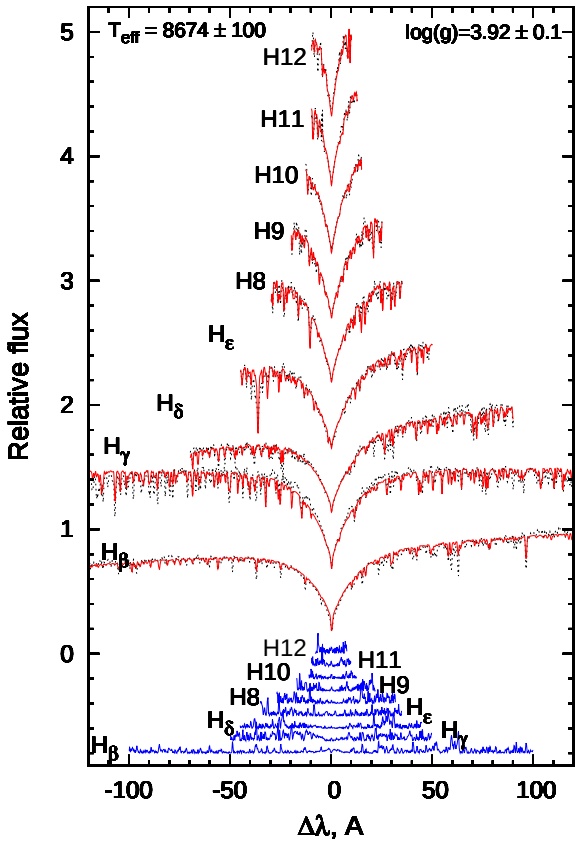

Figure 4. An example of fitting the observed Balmer line profiles (thick line) of HD 27463 by synthetic spectrum (thin dotted line) that corresponds to $T_{\rm eff}$ = 8674 ± 100 K, log g = 3.92 ± 0.10, [M/H]= 0.3 ± 0.1 (χ^2_ν = 1.081). The best fit is obtained for the radial velocity v_r = 22 ± 2 km s^{-1} and vsin i = 27 ± 2 km s^{-1} (see Table 2). Differences between the observed and synthetic profiles are shown at the bottom of this image. The Balmer line profiles are shifted by 0.5 and the differences are shifted by 0.1 for the sake of visibility.

4 STUDY OF FUNDAMENTAL STELLAR PARAMETERS

Some fundamental stellar parameters of HD 27463 were taken from the public astronomical databases (TIC, SIMBAD[4]), (see Tabl. 2). Our estimates of the effective temperature, surface gravity, metallicity, radial velocity and vsin i have been derived by fitting the non-normalised profiles of Balmer lines (see Fig. 4) visible in the two spectra of this star obtained with the spectrograph FEROS operated at the European Southern Observatory (ESO) in La Silla.

We assume here that the high-amplitude periodic variability in the light curve with the lowest frequency and associated first harmonic (see Table 1) corresponds to the stellar rotation. Therefore, we have used the estimate of the stellar radius from the TIC and the spectroscopic value of vsin i to derive the equatorial velocity, $v_{\rm eq}$, and inclination angle, i, of the rotational axis with respect to the line of sight (see Table 2).

[4] simbad.u-strasbg.fr/simbad/sim-id?Ident=HIP19917

Table 2. Fundamental stellar parameters derived for HD 27463.

Parameter	TIC, SIMBAD	This article	
		Balmer lines	Pulsations
$T_{\rm eff}$, K	8669 ± 229	8674 ± 100	8770
log g	3.89 ± 0.33	3.92 ± 0.10	3.887
[M/H]		0.3 ± 0.1	
vsin i, km s^{-1}		27 ± 2	
v_r, km s^{-1}	26.5 ± 4.8[a]	22 ± 2[b]	
$L_\star$, $L_\odot$	38.7 ± 10.8		42.5
$R_\star$, $R_\odot$	2.8 ± 0.4		
$M_\star$, $M_\odot$	2.2 ± 0.4		2.4
$v_{\rm eq}$, km s^{-1}		50 ± 7	40-45
i, deg		33 ± 8	
age, 10^8 years			4.991

Notes: [a] Gontcharov (2006); [b] in barycentric reference frame.

4.1 Analysis of Balmer line profiles

The Balmer line profiles of HD 27463 have been fit employing the FITSB2 code (Napiwotzki et al. 2004). This code uses the grids of synthetic fluxes simulated with the code PHOENIX (Hauschildt et al. 1997) for different values of $T_{\rm eff}$, log g and metallicity. To derive best fit parameters ($T_{\rm eff}$, log g and metallicity) of stellar atmosphere we have employed the code FITSB2 to perform fitting of the Balmer line profiles. During this procedure it takes into account some strong metallic lines that are present at the Balmer wings. The FITSB2 code does not perform an abundance analysis for each chemical element, but it rather results in the estimate of metallicity which serves as an average measure of abundance of metals. For this reason, the spectral lines of most metals are not well fitted in Fig. 4 (see curves for the differences between the synthetic and observed spectra presented at the bottom of this image).

In this study we have used grids of synthetic fluxes[5] simulated by Husser et al. (2013) for models with different metalicities and abundances of the α-elements (O, Ne, Mg, Si, S, Ar, Ca, and Ti) employing the version 16 of the code PHOENIX (Hauschildt & Baron 1999). Husser et al. (2013) have calculated the grids of synthetic fluxes with spectral resolution R=500000, which we reduced to R=50000 when compiled those grids to the format read by the FITSB2 code (Khalack et al. 2017). The resolution used in simulations is close to the spectral resolution of FEROS (see Section 2). Comparing to the PHOENIX15 code, its new version, 16, employs an updated list of atomic and molecular lines and uses a new equation of state to simulate a model of stellar atmosphere and respective synthetic flux (Husser et al. 2013).

The best fit results obtained for one spectrum of HD 27463 are shown in the Table 2 and Fig. 4. The residuals between the synthetic and observed spectra shown in blue in Fig. 4 indicate that the obtained best fit approximates the analysed Balmer line profiles relatively well even taking into account the contamination of Balmer wings by some metal lines. The fitting procedure has been carried out for different values of rotational velocity that allowed us to find the value that minimizes the discrepancy between the observed and simulated Balmer line profiles for vsin i = 27 ± 2 km s^{-1} (see Table 2).

[5] The grids of synthetic spectra are available at http://phoenix.astro.physik.uni-goettingen.de/

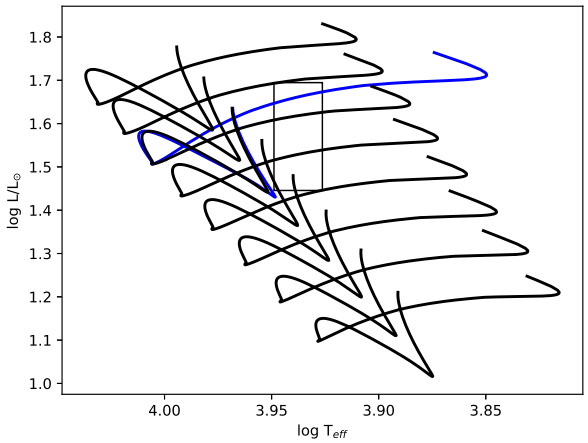

Figure 5. The main sequence evolution tracks for MESA models from 1.9 to 2.6 $M_\odot$, all with zero convective overshoot, are shown in black. The evolution track for the best fitting model with $M_\star$ = 2.4 $M_\odot$, f_{ov} = 0.016, and a ZAMS rotational velocity of 40 km s^{-1} is shown in blue. The box indicates the $1-\sigma$ uncertainty in the observed location of HD 27463.

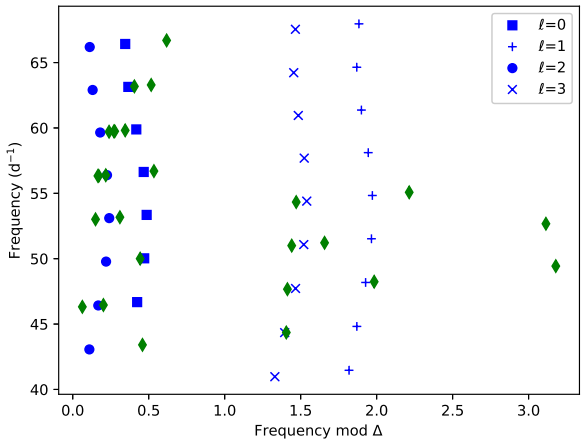

Figure 6. The echelle diagram for the best fitting model and the observed frequencies, both plotted with a large separation of $\Delta\nu = 3.304$ d^{-1}. The blue points show the model frequencies for $\ell = 0$ (squares), $\ell = 1$ (+), $\ell = 2$ (circles), and $\ell = 3$ (x), while the green diamonds specify the data derived from observations. The frequencies plotted here correspond to radial orders of $n = 11 - 19$.

4.2 Analysis of stellar pulsations

We have calculated a grid of stellar structure and evolution models using MESA version 11554 (Paxton et al. 2011, 2013, 2015, 2018, 2019), including the effects of convective overshoot. Model masses ranged from 1.9 to 2.6 $M_\odot$ in 0.1 $M_\odot$ increments, with rotation rates on the ZAMS between 35 and 55 km s^{-1} taking into account the derived value for equatorial velocity (see Table 2). Based on the spectral derivation of metallicity described above, we used a scaled solar metallicity of Z = 0.0244 for all models. Inside the convective core, convective mixing is calculated using the mixing length theory (Böhm-Vitense 1958) with a mixing length $\alpha = 1.73$ (see e.g. Montalbán et al. 2004). Convective overshoot was included above the core using the exponential overshoot model described by Herwig (2000) :

$$D_{ov} = D_0 \exp\left(\frac{-2r}{f_{ov} H_P}\right) \quad (1)$$

where D_0 is the diffusion coefficient at the convective boundary, r is the radial distance from the core boundary, and H_P is the pressure scale height at the core boundary. The amount of overshooting is defined in terms of a fraction of the pressure scale height, H_P. In our models, the amount of overshoot ranged from $f_{ov} = 0$ to 0.04 in increments of 0.01. As many of our best fitting models were found to have overshoot between 0.01 and 0.03, this region of the grid was subsequently refined with steps of 0.002. The models were evolved from the pre-main sequence through the end of the main sequence. Detailed models were saved at least every 20 time steps, and more frequently during certain evolutionary phases. The time steps were variable, and determined by the requirement that the relative change in the stellar structure be less than 10^{-4} from one time step to the next. The evolution tracks for the zero-overshoot models are shown in Figure 5.

We used GYRE (Townsend & Teitler 2013) to calculate linear adiabatic pulsation frequencies for each main sequence model with $3.92 < \log T_{\rm eff} < 3.95$, consistent with both the temperature from the TIC and that derived from the Balmer lines in this work. We calculated model frequencies between 40 and 70 d^{-1} for $\ell = 0$, 1, 2, and 3. Initially, we calculated frequencies for $m = 0$ modes only. Once we had determined a small set of models which were good fits to the observations, we calculated the $\ell = 2$, $m \neq 0$ modes for comparison to the observed rotational splitting.

We used the 26 frequencies from the Table 1, which are greater than 43 d^{-1} to determine large separation, defined as

$$\Delta\nu_0 = < \nu_{n+1,\ell} - \nu_{n,\ell} > . \quad (2)$$

The best fitting large separation is approximately 3.3 d^{-1}, which produces two clear ridges in the echelle diagram, as shown in Fig. 6. We then compared this derived large separation to the values calculated for the models in our grid. The absolute value of the difference between the model and the observed large separation is shown in Fig. 7. A number of models with masses between 2.2 and 2.5 $M_\odot$ have reasonably good fits to the large separation. For models with the smallest difference in the large separation, the echelle diagrams were plotted. Not all models with a large separation of 3.3 d^{-1} were good fits to the observed echelle diagram, so we also compared individual frequency fits, as shown in Fig. 8.

Based on this comparison, our best fitting model was determined to have a large separation of 3.3304 d^{-1}, and is compared to the observations in Fig. 6. This model has a mass of 2.4 $M_\odot$, a ZAMS rotation velocity of either 40 or 45 km s^{-1}, and an overshoot of $f_{ov} = 0.016$. The derived values of effective temperature, $T_{\rm eff} = 8770$ K, and surface gravity, $\log g = 3.887$, are in good agreement with the spectroscopic measurements (see Table 2). The stellar luminosity 42.5 $L_\odot$ derived from the best fitting model is comparable to the value reported in the TIC. The model was determined to have an age of 4.991 $\times 10^8$ years, which corresponds to a core hydrogen fraction of 0.332.

The amount of overshooting we found in this model is similar to that found for KIC 10526294 (Moravveji et al. 2015), and slightly lower than that found for KIC 7760680 (Moravveji et al. 2016). However, both of these stars are late-type B stars, and show g mode pulsations typical of Slowly Pulsating B (SPB) stars. Similar studies of a magnetic B-type star (HD 43317) found a much

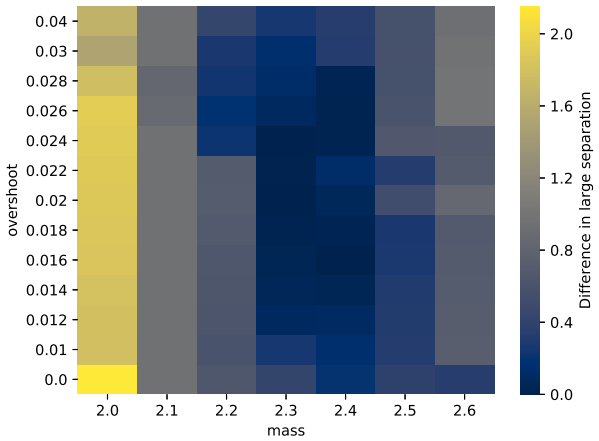

Figure 7. The absolute value of the difference in the large separation for the models in our grid compared to the observed value, shown as a function of mass and overshoot. Based on the difference in the large separation and comparison to echelle diagrams, the best fitting model was determined to have $M_\star = 2.4$ M$_\odot$ and $f_{ov} = 0.016$.

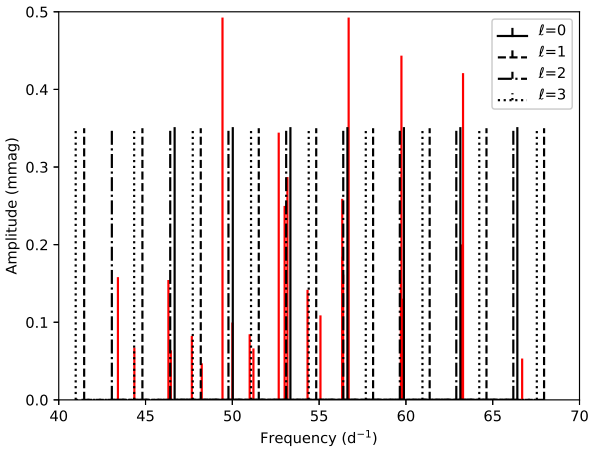

Figure 8. Individual frequency matches for the best fitting model. The red lines are the observed frequencies plotted versus amplitude, while the black lines are the $\ell = 0$ (solid), $\ell = 1$ (dashed), $\ell = 2$ (dot-dashed), and $\ell = 3$ (dotted) model frequencies.

lower convective overshoot ($f_{ov} = 0.004$) and the authors conclude that the convective mixing is suppressed by the magnetic field (Buysschaert et al. 2018).

Once we had established a best fitting model, we calculated rotational splitting in the $\ell = 2$ modes to see if this provided matches for some of the unmatched frequencies in the echelle diagram. As shown in Fig. 9, the observed mode splitting agrees well with our model calculations. For a model that is initially rotating at 40 km s^{-1}, the rotation rate has dropped to 18.8 km s^{-1} ($\Omega/\Omega_{crit} = 0.048$) at $X_c = 0.332$. Based on these calculations, we present our best fitting mode identification in Table 1.

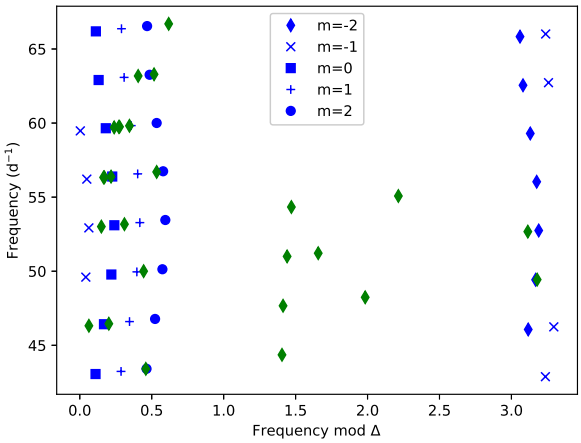

Figure 9. The mode splitting in the $\ell = 2$ mode for the best fitting model. The $m = -2$, -1, 0, 1, and 2 frequencies are denoted by diamonds, x, squares, +, and o respectively. The green diamonds indicate the observed frequencies. The range of radial orders shown is the same as in Fig. 6.

5 DISCUSSION

The detected photometric variability of HD 27463 with the period P= 2.834274 $\pm$ 0.000008 d (see Table 1 and Fig. 3) can be explained in terms of axial stellar rotation within the oblique magnetic rotator model (Stibbs 1950). In a hydrodynamically stable stellar atmosphere even a relatively weak magnetic field can amplify the atomic diffusion and lead to horizontal and vertical stratification of chemical abundances (Alecian & Stift 2010; Stift & Alecian 2012, 2016). Usually the magnetic CP stars host magnetic fields that are dominated by a dipolar component with strengths on the order of several kG or less, which remains stable over long timescales (Silvester et al. 2014; Kochukhov et al. 2019). The magnetically sensitive line profiles Fe II 6147Å, 6149Å visible in the FEROS spectra of HD 27463 are not visually split due to the Zeeman effect. Therefore, it seems that the magnetic field is not very strong in the stellar atmosphere of this star and might be of order of a few hundred Gauss. Nevertheless, it is still significant enough to cause the formation of abundance patches in the stellar atmosphere of this star taking into account its spectral classification as an Ap EuCr(Sr) star (Houk & Cowley 1975). The patches of enhanced abundance of different metals usually are located close to the magnetic poles or along the magnetic equator (Lüftinger et al. 2010; Kochukhov et al. 2019; Mathys & Khalack 2019) and contribute to the variability of spectral line profile and photometric flux with the phase of axial stellar rotation. Assuming the oblique magnetic rotator model in the case of HD 27463 the overabundance patches located at the magnetic poles will generate a signal at the first harmonic of the rotational frequency. The derived pattern of stellar variability in the low frequency domain is in a good accordance with the predictions of the oblique magnetic rotator model (see Fig. 3).

The lower panel at the Fig. 3 indicates that HD 27463 shows high-frequency pulsations at the spectral region from 40 to 70 d^{-1} with amplitudes less than 0.5 mmag. Such high-frequency pulsation modes are typically found in hotter δ Scuti stars (Smalley et al. 2017; Bowman & Kurtz 2018a). This is because the heat-engine driving mechanism operating in the He II ionisation zone is closer to the surface and is more efficient at exciting higher radial orders,

hence higher frequencies, in hotter δ Scuti stars (Pamyatnykh 2000; Dupret et al. 2019). Cunha et al. (2019) and Sikora et al. (2019) have also classified this star as a suspected δ Scuti variable. Therefore, our spectroscopic parameters and subsequent modelling results are in agreement with this theoretically predicted and observed relationship.

The δ Scuti stars are known to show a long-term variability of their pulsation amplitudes and frequencies (Breger 2000; Bowman 2016). To study possible amplitude variability in HD 27463, we employed the methodology of Bowman et al. (2016), such that the amplitude and phase of a pulsation mode was tracked at fixed frequency using linear least-squares throughout the *TESS* light curve. To achieve this, the *TESS* light curve of HD 27463 was divided into bins of 50 d with a step of 1 d, and amplitude and phase of a pulsation mode were optimized using linear least-squares in each bin for the frequency determined using the entire light curve. In our analysis, the zero-point of the time used in the calculation of phases was chosen as the approximate midpoint of the entire *TESS* light curve (i.e. BJD 2471340.0). The 1-σ uncertainties for the amplitude and phase values were obtained from the least-squares fit.

Employing this technique we were able to detect marginal amplitude and phase modulation given the relatively large uncertainties for the pulsation modes in HD 27463. An example of the amplitude and phase modulation for the pulsation mode frequency at 59.2474 d^{-1} is shown in Fig. 10. Other pulsation modes with a relatively high amplitudes (see Table 1) show similar behaviour. Our detection of amplitude and phase modulation for pulsation modes with relatively high amplitudes is in agreement with the findings of Bowman et al. (2016) that amplitude modulation is common in δ Scuti stars with long-term amplitude modulation occurring on time scales much longer than the rotation period. Such long-term amplitude modulation is not observed in roAp stars (see Cunha et al. 2019). Some pulsation modes in HD 27463 have quite small amplitudes. In this case, it is difficult to search for an amplitude modulation taking into account that the error-bars derived from a non-linear least squares fit are of order 0.01 mmag.

We have also analysed the 26 frequencies of detected stellar pulsations located in the frequency range between 40 and 70 d^{-1} (see Table 1) that result in the best fitting large separation around 3.3 d^{-1} which is used as constraint in modelling of pulsation modes (see Fig. 6). The grid of stellar evolution models has been calculated with MESA version 11554 (Paxton et al. 2011, 2013, 2015, 2018, 2019) including the effects of convective overshoot, while the simulation of linear adiabatic pulsation frequencies for each main sequence model has been carried out using the code GYRE (Townsend & Teitler 2013). Our best fitting model corresponds to the overshoot of $f_{ov} = 0.016$ and results in the values of global stellar parameters that are very close to those reported in the TIC and to those derived in this paper from the simulation of Balmer line profiles (see Table 2). This model was determined to have an age of 4.991 $\times 10^8$ years, which corresponds to a core hydrogen fraction of 0.332.

We have found that the large separation is not a sensitive function of the convective core overshoot, as shown in Fig. 7. The large separation serves to narrow down the number of models, which must then be compared to the observed echelle ridges (see Figs. 6, 9) and the individual frequencies (see Fig. 8) to determine the best fitting parameters.

The radial orders inferred from this work are high for δ Scuti stars, which are typically observed to have low ($1 \leq n \leq 7$) radial orders. It has been shown by Antoci et al. (2014) that moderate ($7 \leq n \leq 15$) radial orders can be excited in δ Scuti stars by means of

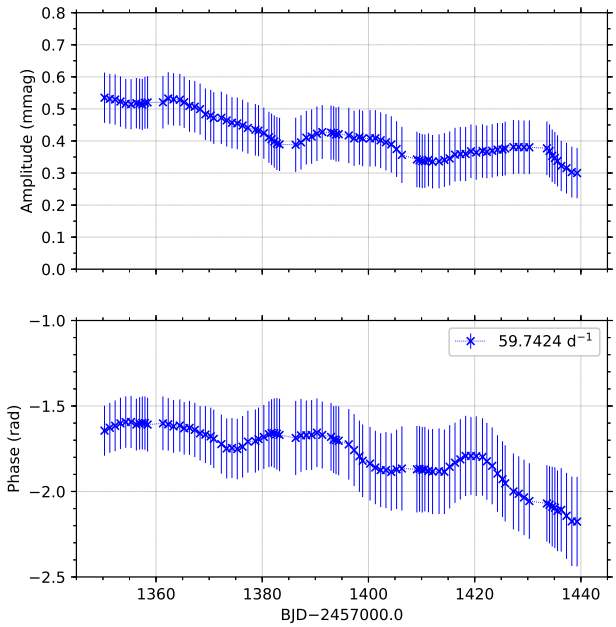

Figure 10. Variability of the amplitude and phase with time for stellar pulsation detected at the frequency ν = 59.7424 d^{-1}. 1-σ uncertainties are determined from the least-squares fit.

turbulent pressure, although this pulsation excitation mechanism is most efficient in the centre of the classical instability strip. HD 27463 has been shown in this work to be closer the predicted blue edge of the classical instability strip instead of the centre, with an effective temperature of approximately 8600 K.

For chemically-peculiar stars, the presence of a strong large-scale magnetic field is expected to suppress the kappa mechanism and the excitation of low-radial order pressure modes (Saio 2005). Instead, the excitation of high-radial order magneto-acoustic modes are expected and observed in roAp stars. The detection of rotationally-split multiplets of non-radial pulsation modes with high radial orders in a (magnetic) chemically-peculiar star is the discriminating factor between roAp and δ Scuti stars. Therefore the determination of the exact driving mechanism in HD 27463 requires the (non-)detection of a strong large-scale magnetic field in HD 27463, but this is beyond the scope of the present work. Nonetheless, the rich frequency spectrum of HD 27463 including radial and non-radial modes spanning several radial orders demonstrates the exciting prospects for asteroseismic studies of intermediate-mass stars with TESS.

ACKNOWLEDGMENTS

V.K., C.L. and A.D.U. acknowledge support from the Natural Sciences and Engineering Research Council of Canada (NSERC). O.K. and V.K. are thankful to the Faculté des Études Supérieures et de la Recherch and to the Faculté des Sciences de l'Université de Moncton for the financial support of this research. This paper includes data collected by the *TESS* mission. Funding for the *TESS* mission is provided by the NASA Explorer Program. Funding for the TESS Asteroseismic Science Operations Centre is provided by the Danish National Research Foundation (Grant agreement no.: DNRF106), ESA PRODEX (PEA 4000119301) and Stellar Astrophysics Centre (SAC) at Aarhus University. We thank the *TESS* and TASC/TASOC

teams for their support of the present work. This research has made use of the SIMBAD database, operated at CDS, Strasbourg, France. Some of the data presented in this paper were obtained from the Mikulski Archive for Space Telescopes (MAST). STScI is operated by the Association of Universities for Research in Astronomy, Inc., under NASA contract NAS5-2655. The research leading to these results has received funding from the European Research Council (ERC) under the European Union's Horizon 2020 research and innovation programme (grant agreement No. 670519: MAMSIE). This study is also partially based on data obtained from the ESO Science Archive Facility under request number Khalack399537.

REFERENCES

Aerts C., Molenberghs G., Michielsen M., Pedersen M.G., Björklund R., Johnston C., Mombarg J.S.G., Bowman D.M., et al. 2018, ApJS, 237, 15
Alecian G., Stift M.J., 2010, A&A, 516, 53
Antoci V., Cunha M., Houdek G., Kjeldsen H., Trampedach R., Handler G., Lüftinger T., Arentoft T., et al. 2014, ApJ, 796, 118
Babcock H.W., 1958, ApJ, 128, 228
Baize P., Petit M., 1989, A&AS, 77, 497
Böhm-Vitense E., 1958, Zeitschrift fur Astrophysik, 46, 108
Bowman D.M., Kurtz D.W., 2018a, MNRAS, 476, 3169
Bowman D.M., Buysschaert B., Neiner C., Pápics P.I., Oksala M.E., Aerts C., 2018b, A&A, 616, A77
Bowman D.M., 2016, PhD thesis, Jeremiah Horroks Institute, University of Central Lancashire, UK
Bowman D.M., Kurtz D.W., Breger M., Murphy S.J., Holdsworth D.L., 2016, MNRAS, 460, 1970
Breger M., 2000, MNRAS, 313, 129
Buysschaert B., Aerts C., Bowman D.M., Johnston C., Van Reeth T., Pedersen M.G., Mathis S., Neiner C., 2018, A&A, 616, A148
Campante T.L., Schofield M., Kuszlewicz J.S. et al., 2016, ApJ, 830, 138
Cleveland W.S., 1979, Journal of the American Statistical Association, 74, N368, 829
Cunha M.S., Antoci V., Holdsworth D.L., Kurtz D.W., Balona L. A., Bognár Zs., Bowman D.M. , Guo Z. et al., 2019, MNRAS, accepted
David-Uraz A., Neiner C., Sikora J., Bowman D.M., Petit V., Chowdhury S., Handler G., Pergeorelis M., et al., 2019, MNRAS, accepted, arXiv:1904.11539
Dupret M.A., Grigahcène A., Garrido R., Gabriel M., Scuflaire R., 2004, A&A, 414, L17
Gontcharov G.A., 2006, PAZh, 32, 844
Hauschildt P. H., Baron E., Allard F., 1997, ApJ, 483, 390
Hauschildt P. H., Baron E., 1999, JCoAM, 109, 41
Herwig F., 2000, A&A360, 952
Holdsworth D.L., Cunha M.S., Shibahashi H., Kurtz D.W., Bowman D.M., 2018, MNRAS, 480, 2976
Holdsworth D.L., Kurtz D.W., Smalley B., Saio H., Handler G., Murphy S.J., Lehmann H., 2016, MNRAS, 462, 876
Holdsworth D.L., Smalley B., Gillon M., Clubb K.I., Southworth J., Maxted P.F.L., Anderson D.R., Barros S.C.C, et al., 2014, MNRAS, 439, 2078
Houk N., Cowley A.P., 1975, Michigan Spectral Survey, 1, 0
Husser T.-O., Wende-von Berg S., Dreizler S. et al., 2013, A&A, 553, 6
Jenkins 2016, Proc. SPIE 9913, Software and Cyberinfrastructure for Astronomy IV, 99133E
Joshi S., Martinez P., Chowdhury S. et al., 2016, A&A, 590, A116
Kaufer A., Stahl O., Tubbesing S., Nørregaard P., Avila G., Francois P.,Pasquini L., Pizzella A., 1999, Messenger, 95, 8
Khalack V., LeBlanc F., 2015a, AJ, 150, 1, id.2
Khalack V., LeBlanc F., 2015b, Advances in Astronomy and Space Physics, 5, 3
Khalack V., Gallant G., Thibeault C., 2017, MNRAS, 471, 926
Kochukhov O., Shultz M., Neiner C., 2019, A&A, 621, 47K
Kurtz D.W., 1978, IBVS, 1436, 1
van Leeuwen F., 2007, A&A, 474, 653
Lenz P., Breger M., 2005, Commun. in Asteroseismology, 146, 53
Lüftinger T., Fröhlich H.-E., Weiss W.W., Petit P., Aurière M., Nesvacil N., Gruberbauer M., Shulyak D., et al. 2010, A&A, 509, 43L
Martinez P., Kurtz D.W., 1994, MNRAS, 271, 129
Mathys G., Khalack V., 2019, in preparation
Maury A.C., Pickering E.C., 1897, Annals of Harvard College Observatory, 28, 1
Montalbán J., D'Antona F., Kupka F., Heiter U., 2004, A&A, 416, 1081
Montgomery M.H., Odonoghue D., 1999, Delta Scuti Star Newsletter, 13, 28
Moravveji E., Townsend R.H.D., Aerts C., Mathis S., 2016, ApJ, 823, 130
Moravveji E., Aerts C., Pápics P.I., Triana S.A.,Vandoren B., 2015, A&A, 580, A27
Napiwotzki R., Yungelson L., Nelemans G., Marsh T. R., Leibundgut B., Renzini R., Homeier D., Koester D. et al., 2004, in: Hilditch R. W., Hensberge H. & Pavlovski K., eds, ASP Conf. Ser. Vol. 318, Spectroscopically and Spatially Resolving the Components of the Close Binary Stars, San Francisco, p. 402
Pamyatnykh A.A., 2000, in: Breger M., Montgomery M., eds, Astronomical Society of the Pacific Conference Series Vol. 210, Delta Scuti and Related Stars, p. 215
Paxton B., Smolec R., Schwab J., Gautschy A., Bildsten L., Cantiello M., Dotter A., Farmer R.,et al. 2019, ApJS, accepted, arXiv:1903.01426
Paxton B., Schwab J., Bauer E.B., Bildsten L., Blinnikov S., Duffell P., Farmer R., Goldberg J.A. et al., 2018, ApJS, 234, 34
Paxton B., Marchant P., Schwab J., Bauer E.B., Bildsten L., Cantiello M., Dessart L., Farmer R. et al., 2015, ApJS, 220, 15
Paxton B., Cantiello M., Arras P., Bildsten L., Brown E.F., Dotter A., Mankovich C., Montgomery M.H. et al, 2013, ApJS, 208, 4
Paxton B., Bildsten L., Dotter A., Herwig F., Lesaffre P., Timmes F., 2011, ApJS, 192, 3
Ricker G.R., Winn J.N., Vanderspek R. et al., 2015, Journal of Astronomical Telescopes, Instruments and Systems, 1, 014003
Ricker G., Vanderspek R., 2018, doi:10.17909/t9-wx1n-aw08
Saio H. 2005, MNRAS, 360, 1022
Seabold S., Perktold J., 2010, in van der Walt S. & Millman J., eds, Proc. of the 9th Python in Science Conference, p. 62
Shultz M.E., Wade G.A., Rivinius Th., Neiner C., Alecian E., Bohlender D., Monin D., Sikora J. 2018, MNRAS, 475, 5144
Silvester J., Kochukhov O., Wade, G.A. 2014, MNRAS, 440, 182
Sikora J., David-Uraz A., Chowdhury S., Bowman D.M., Wade G.A., Khalack V., Kobzar O., Kochukhov O., et al., 2019, MNRAS, submitted
Smalley B., Antoci V., Holdsworth D.L., Kurtz D.W., Murphy S.J., De Cat P., Anderson D.R., Catanzaro G., et al. 2017, MNRAS, 465, 2662
Stassun K.G., Oelkers R.J., Pepper J. et al., 2018, AJ, 156, 102
Stibbs D.W.N. 1950, MNRAS, 110, 395
Stift M.J., Alecian G., 2012, MNRAS, 425, 2715
Stift M.J., Alecian G., 2016, MNRAS, 457, 74
Townsend R.H.D., Teitler S.A., 2013, MNRAS, 435, 3406